Kylin 1.0: An *Ab-Initio* Density Matrix Renormalization Group Quantum Chemistry Program

Zhaoxuan Xie[*], Yinxuan Song[*], Fangwen Peng[*], Jianhao Li[*], Yifan Cheng[*], Lingzhi Zhang[*], Yingjin Ma[†], Yingqi Tian[*‡], Zhen Luo[*§], Haibo Ma[¶‖]

November 29, 2022

Abstract

The accurate evaluation of electron correlations is highly necessary for the proper descriptions of the electronic structures in strongly correlated molecules, ranging from bond-dissociating molecules, polyradicals, to large conjugated molecules and transition metal complexes. For this purpose, in this paper, a new *ab-initio* quantum chemistry program Kylin 1.0 for electron correlation calculations at various quantum many-body levels, including configuration interaction (CI), perturbation theory (PT), and density matrix renormalization group (DMRG), is presented. In addtion, fundamental quantum chemical methods such as Hartree-Fock self-consistent field (HF-SCF) and the complete active space SCF (CASSCF) are aslo implemented. The Kylin 1.0 program possesses these features: (1) efficient DMRG implementation based on the matrix product operator (MPO) formulation for describing static electron correlation within a large active space composed of more than 100 orbitals, supporting both $U(1)_n \times U(1)_{S_z}$ and $U(1)_n \times SU(2)_S$ symmetries; (2) efficient second-order DMRG-self-consistent field (SCF) implementation; (3) externally-contracted multi-reference CI (MRCI) and Epstein-Nesbet PT with DMRG reference wave functions for including the remaining dynamic electron correlation outside the large active spaces. In this paper, we introduce the capabilities and numerical benchmark examples of the Kylin 1.0 program.

[*]School of Chemistry and Chemical Engineering, Nanjing University, Nanjing 210023, China

[†]Computer Network Information Center, Chinese Academy of Sciences, Beijing 100190, China

[‡]tianyq@nju.edu.cn

[§]luozhen@nju.edu.cn

[¶]Qingdao Institute for Theoretical and Computational Sciences, Qingdao Institute of Frontier and Interdisciplinary Science, Shandong University, Qingdao 266237, China

[‖]haibo.ma@sdu.edu.cn

1 INTRODUCTION

Nowadays the accurate computation of the electronic structures in large and strongly correlated chemical systems is one of the main challenges in the quantum chemistry community.[1–5] Here, the strong correlation refers to the situation in many chemical problems such as bond breaking/formation in chemical reactions and transition metal catalysis in biological photosynthesis, in which there are many energetically near-degenerate frontier molecular orbitals (MOs), making it impossible to approximate the electronic wavefunction by using only one leading component. In such cases, usually a limited number of possible and important Slater determinants (SDs) or configuration state functions (CSFs) have to be first identified. For example, the widely used complete active space (CAS) methods expand the electronic wavefunction using all possible SDs or CSFs within an active space constructed from a limited number of pre-selected active orbitals. Unfortunately, it is infeasible to obtain the exact full configuration interaction (FCI) solution for large active spaces, as the dimension of the configuration space grows exponentially with the increasing system size. Nowadays, the largest exactly solvable active space is 20 electrons in 20 orbitals, i.e. (20e, 20o).

In order to break through the above limitation of small active space (also known as "curse of dimensionality"), various multi-configurational quantum chemistry methods have been proposed to achieve near-exact FCI solution, such as FCI quantum Monte Carlo (FCIQMC)[6], perturbatively selected configuration interaction (CIPSI)[7], heat-bath configuration interaction (SHCI)[8,9], iterative CI with selection (iCI)[10,11], etc. Among them, the density matrix renormalization group (DMRG) method[12–15] has become one of the biggest breakthroughs in quantum chemistry in the last quarter century to tackle the challenge of simulating strongly correlated molecules.[16–21] DMRG's great success can be ascribed to its efficient compression and localized representation of quantum states in its wave function's entangled matrix product state (MPS) formulation or the equivalent tensor train (TT) structure in mathematical language.[22] DMRG is now widely used as a benchmark reference when testing new quantum chemical methods for strong electron correlation problems, and it also evolves from a purely approximate FCI solver to being fully adapted to a variety of CAS and multi-reference (MR) methods.[23–28]

Currently, there are three publicly available and popular *ab-initio* DMRG programs: BLOCK/BLOCK2 by the Chan group[29], QCMAQUIS by the Reiher group[20,30] and CheMPS2 by Wouters et al.[31]. These programs include efficient and highly scalable implementation of DMRG for quantum chemistry, and provide powerful platforms for production level calculation of realistic systems and new algorithm development. In the meantime, all of these three DMRG programs require precalculated two-electron integrals and information about the active orbital space. Therefore, a general-purpose quantum chemistry programs is usually involved, or the DMRG calculation is performed employing an interface between a DMRG code and a general-purpose program, such as PySCF[32,33] or OpenMolcas[34]. In addition, the formulation of DMRG wave functions is intuitively quite different from that of traditional quantum chemical multi-configurational wave functions, hindering the application of traditional wave function analysis tools for the users' convenient understanding of the electronic structure features. Moreover, to achieve highly quantitative accuracy for practical molecular systems, it is desirable to implement post-DMRG treatments to include nonnegligible electron correlations between CAS and all other (about a few hundreds or thousands of) inactive MOs (including core orbitals and external orbitals), i.e., dynamic electron correlation caused by the instantaneous movement of the electrons.[28]

In this work, we introduce a new *ab-initio* DMRG program, Kylin 1.0, which can be used as an independent quantum chemical software, with no necessity to involve additional packages. Through utilizing a second-generation DMRG language based on MPS and matrix product operator (MPO), Kylin 1.0 aims to provide an advanced platform for efficient *ab-initio* DMRG calculations of large sized active spaces with up to more than 100 active orbitals (when using a standalone server). In order to make the *ab-initio* DMRG program easy-to-use, Kylin 1.0 also features extensive capabilities in pre-DMRG and post-DMRG treatments, including Hartree-Fock self-consistent field (HF-SCF) and the complete active space SCF (CASSCF), single-reference and multi-reference CI, single-reference and multi-reference PT as well as DMRG wave function analysis and geometry optimization. All of the available methodologies in the Kylin 1.0 package are illustrated in Fig. 1. Kylin 1.0 is free of charge for academic users and distributed commercially to industry via the website (http://kylin-qc.com). We will give brief introductions to these methods in Section 2, as well

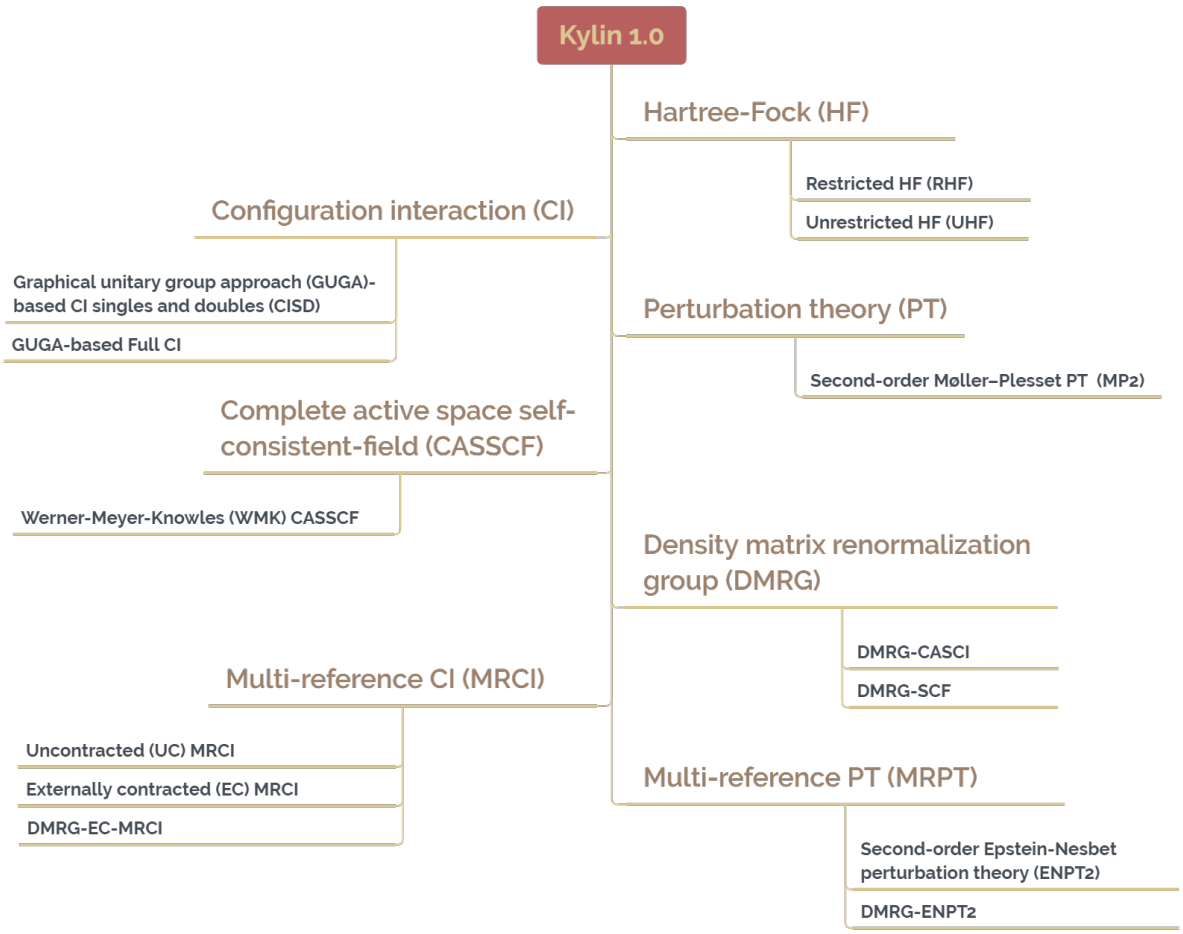

Figure 1: Implemented methodologies in Kylin 1.0.

as some technique features in Section 3. Then we present numerical examples and discussions in Section 4, and a short summary and outlook in Section 5.

2 METHODOLOGY

2.1 Hartree-Fock SCF, Configuration Interaction and Perturbation Theory

Most *ab-initio* methods build many-electron wave functions from atomic orbitals (AOs) or MOs. The simplest many-electron wave functions constructed from MOs are obtained from

Hartree-Fock SCF calculation at a mean field level. In Kylin 1.0 package, restricted and unrestricted Hartree-Fock (RHF and UHF) approaches[35–37] are implemented with AO integrals from integral library libcint[38]. Techniques including Pulay's direct inversion in the iterative subspace (DIIS)[39], C2-DIIS[40] and energy-DIIS (EDIIS)[41] are optional to accelerate SCF convergence. Abelian point group symmetries up to D_{2h} can be identified automatically in principal axis systems and symmetry-adapted orbital integrals are determined using double coset[42].

To recover the electron correlation energy, which is absent in HF method due to the single configuration approximation, the post-HF methods are necessary. One possible solution is CI method, whose wavefunction is constructed as a linear combination of configurations. The CI singles-and-doubles (CISD) and full CI (FCI) methods are implemented in Kylin 1.0. The CISD wavefunction includes HF configuration as well as its single and double excitation configurations, while the FCI wavefunction further includes all other higher excitation configurations. The CISD and FCI calculations are performed by the graphical unitary group approach (GUGA),[43–48] where the CSF is represented by a complete walk from top vertex to bottom vertex in the shavitt graph.[46–48] The spin-free Hamiltonian can be written as

$$\hat{H} = \sum_{pq} h_{pq}\hat{E}_{pq} + \frac{1}{2}\sum_{pqrs}(pq|rs)\hat{e}_{pq,rs}, \tag{1}$$

where

$$h_{pq} = \langle p|\hat{h}|q\rangle \tag{2}$$

and

$$(pq|rs) = \langle p(1)r(2)|\frac{1}{r_{12}}|q(1)s(2)\rangle \tag{3}$$

are the one-electron and two-electron MO integrals, and p, q, r, s represent the MOs.

$$\hat{E}_{pq} = \sum_{\sigma}\hat{c}^{\dagger}_{p\sigma}\hat{c}_{q\sigma} \tag{4}$$

and

$$\hat{e}_{pq,rs} = \hat{E}_{pq}\hat{E}_{rs} - \delta_{qr}\hat{E}_{ps} \tag{5}$$

are the one-body and two-body unitary group operators, where $\hat{c}^{\dagger}_{p\sigma}$ and $\hat{c}_{q\sigma}$ are the electron creation and annihilation operators acting on the pth and qth orbitals with spin σ

respectively. The problem of constructing Hamiltonian matrix is thus reduced to the problem of calculating the matrix elements of these unitary group operators. Since a unitary group operator matrix element forms a loop in the shavitt graph (e.g. Fig. 3 in Ref[48]), the loop-driven algorithm[45,46] is performed, which avoids duplicate matrix elements calculation. In addition, the direct CI algorithm[49,50] is also implemented in order to avoid storage of Hamiltonian matrix elements especially for large-scale CI calculations.

Another widely-used post-HF method, the second-order Moller-Plesset perturbation theory (MP2)[51], is also available in Kylin 1.0. The MP2 method uses the sum of Fock operators as the zeroth-order Hamiltonian, and adds the correlation energy beyond the HF by means of Rayleigh–Schrodinger perturbation theory (RSPT):

$$E_0^{(2)} = \frac{1}{4}\sum_{pqrs}\frac{(pr||qs)(qs||pr)}{\epsilon_p + \epsilon_q - \epsilon_r - \epsilon_s}, \tag{6}$$

where $(pr||qs) = (pr|qs) - (ps|qr)$, and ϵ_p is the orbital energy. The indices p and q refer to spin orbitals that are occupied in the reference function, and the labels r and s refer to spin orbitals that are unoccupied in the reference function (virtual orbitals). For those systems where a single determinant can be utilized as a reasonable reference, the MP2 method usually describes the missing electron correlation energy satisfactorily.

2.2 DMRG

The main function of Kylin 1.0 is its DMRG calculation for large active spaces with a few tens or even more than 100 active orbitals. By using the MPS ansatz, the expansion of the DMRG wave function of a L-orbital system can be written as

$$|\psi\rangle = \sum_{n_1\cdots n_L} M^{n_1}_{1a_1} M^{n_2}_{a_1a_2}\cdots M^{n_L}_{a_{L-1}1}|n_1\cdots n_L\rangle \tag{7}$$

in which $|n_1\cdots n_L\rangle$ is the occupation-number representation of the configuration, and $M^{n_i}_{a_{i-1}a_i}$ represents an element of the local rank-3 tensor $M[i]$, which has two link bonds a_{i-1}, a_i with dimensions m_{i-1}, m_i and one physical bond n_i with dimension d (the number of possible occupations of orbital i). For simplicity, it is assumed that the dimensions of all link bonds m_i are the same m (dimension parameter). Similarly, one can decompose the global operator

$\widehat{O}$ to the MPO tensors,

$$\widehat{O} = \sum_{\substack{n_1 \cdots n_L \\ n_1^* \cdots n_L^*}} W_{1b_1}^{n_1^* n_1} W_{b_1 b_2}^{n_2^* n_2} \cdots W_{b_{L-1}1}^{n_L^* n_L} |n_1^* \cdots n_L^*\rangle\langle n_1 \cdots n_L| \tag{8}$$

in which $W_{b_{i-1}b_i}^{n_i^* n_i}$ represents an element of the local rank-4 tensor $W[i]$, which has two link bonds b_{i-1}, b_i with dimensions D_{i-1}, D_i and two physical bonds n_i, n_i^*. The ground state energy ϵ can be minimized by introducing the Lagrange multiplier

$$\mathcal{L} = \langle\psi|\widehat{H}|\psi\rangle - \epsilon\left(\langle\psi|\psi\rangle - 1\right) \tag{9}$$

and solving the equation

$$\frac{\partial\mathcal{L}}{\partial M_{a_{k-1}a_k}^{n_k^*}} = \frac{\partial}{\partial M_{a_{k-1}a_k}^{n_k^*}}\langle\psi|\widehat{H}|\psi\rangle - \epsilon\frac{\partial}{\partial M_{a_{k-1}a_k}^{n_k^*}}\langle\psi|\psi\rangle = 0 \tag{10}$$

site-by-site from one end of the chain of sites to the other. Since we have decomposed both the wavefunction and the operator in Eq. 10, and the unitarity of the matrix $M_{a_{i-1}a_i}^{n_i}$ is ensured by the singular value decomposition (SVD) procedure, the first derivatives on the right side of Eq. 10 can be easily computed because of $M^{n_i^*}M^{n_i} = 1$. By optimizing each local component $M_{a_{i-1}a_i}^{n_i}$ of $|\psi\rangle$ and sweeping sites until convergence, the minimization in Eq. 9 is achieved, resulting in $|\psi\rangle$. The decomposed MPS and MPO can be represented in tensor network form as illustrated in Fig. 2.

If the Hilbert space $\mathcal{H}$ and Hamiltonian $\widehat{H}$ is protected by some on-site symmetries of group G (e.g. charge, spin conservation and Abelian point group symmetries of molecules), one can partition a physical bond $|n_i\rangle$ into different irreducible representations labelled with some quantum numbers q_{n_i}. Due to properties of density matrices (quasi-density matrices in spin-adapted case), similarly a link bond $|a_i\rangle$ can be divided into subspaces labelled with q_{a_i}. According to group representation theory, for such a symmetry-protected tensor, the product of irreducible representations of all input bonds must equal to that of output bonds, otherwise the tensor elements would simply vanish. Therefore, symmetry-protected tensors can be arranged in a block-sparse format considering only the non-zero tensor blocks. Moreover, for non-Abelian symmetries such as $\mathrm{SU}(2)_\mathrm{S}$, if we consider an A-tensor labelled with spin irreducible representations S and its components S_z, the Wigner-Eckart theorem

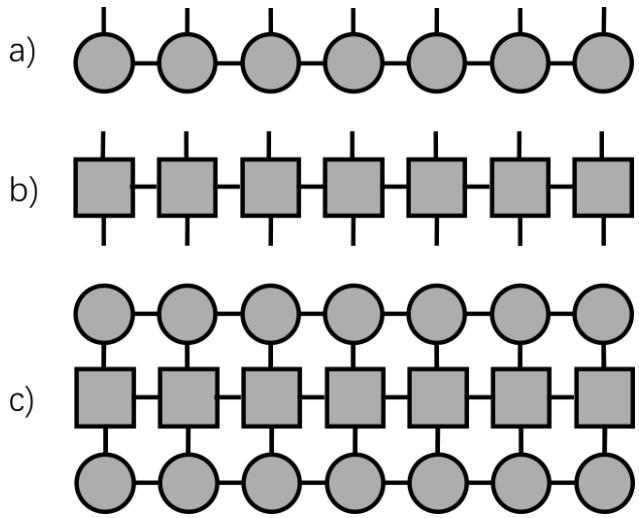

Figure 2: The tensor network for MPS, MPO and $\langle\psi|\widehat{H}|\psi\rangle$. a) Decomposed wave function as MPS. Each dot represent a rank-3 tensor $M^{n_i}_{a_{i-1}a_i}$. b) Decomposed operator as MPO. Similar to MPS, each block represent a rank-4 tensor $W^{n_i^* n_i}_{b_{i-1}b_i}$. c) The $\langle\psi|\widehat{H}|\psi\rangle$ operation in tensor network form. Each linked bond means that the two linked tensors should be contracted.

indicates that A can be divided into two parts

$$\left(A^{n_i}_{a_{i-1}a_i}\right)^{S_{n_i}S^z_{n_i}}_{S_{a_{i-1}}S^z_{a_{i-1}}S_{a_i}S^z_{a_i}} = \left(A^{n_i}_{a_{i-1}a_i}\right)^{S_{n_i}}_{S_{a_{i-1}}a_i} C^{S_{a_{i-1}}\ S_{n_i}\ S_{a_i}}_{S^z_{a_{i-1}}\ S^z_{n_i}\ S^z_{a_i}} \tag{11}$$

which $\left(A^{n_i}_{a_{i-1}a_i}\right)^{S_{n_i}}_{S_{a_{i-1}}S_{a_i}}$ are reduced matrix elements independent of component S_z and $C^{S_{a_{i-1}}\ S_{n_i}\ S_{a_i}}_{S^z_{a_{i-1}}\ S^z_{n_i}\ S^z_{n_i}}$ is Clebsch-Gordan coefficient. Therefore, tensors are arranged in a even more compact format considering only the reduced elements and Clebsch-Gordan coefficients occur only during tensor contraction.

It should be noted that, the DMRG convergence is largely affected by the orbital ordering, due to the sequential nature of the sweeping optimization of MPS local tensors. In the Kylin 1.0 package, we implement an orbital reordering procedure based on the widely used graph theory technique. By constructing an undirected graph between all orbitals and using the absolute values of the exchange integrals as the weights of the edges, we can easily get an optimized orbital order by computing the Fiedler vector of this graph.

2.3 CASSCF and DMRG-SCF

Since multi-configurational wave functions depend greatly on the choice of selected MOs in an active space, a CASSCF calculation is usually performed, in which both CI coefficients and MO coefficients are optimized simultaneously by minimizing the total energy. In quantum chemistry calculations, a set of MOs $\{\phi_i\}$ are usually represented as a linear combinations of AOs $\{\chi_\mu\}$, as

$$\phi_i = \sum_{\mu=1}^{m} C_\mu^i \chi_\mu. \tag{12}$$

To minimize the total energy while maintaining the orthogonality of MOs, one can perform an unitary transformation $\mathbf{U}$ on the MO coefficient matrix $\mathbf{C}$, as

$$\mathbf{C} = \mathbf{C}_0\mathbf{U}, \tag{13}$$

where $\mathbf{C}_0$ is the matrix containing initial MO coefficients, and usually comes from Hartree-Fock calculations; while the unitary matrix $\mathbf{U}$ can be obtained from the SCF procedures in CASSCF calculations. The total energy E in the CASSCF method can be computed with

$$E = \sum_{tu} \langle t|\hat{h}|u\rangle \gamma_{tu} + \frac{1}{2}\sum_{tuvw} (tu|vw)\Gamma_{tuvw} + E_{core} \tag{14}$$

in which γ_{kl} and Γ_{mnkl} are respectively one- and two-electron reduced density matrices (RDMs), and E_{core} is a constant containing energies from nuclear repulsion and frozen core electrons. Since the MO integrals $\langle t|\hat{h}|u\rangle$ and $(tu|vw)$ depend only on the orbital coefficients when the molecular geometry stays fixed, it is clear that the total energy E depends both on the CI coefficients $\mathbf{c}$ and the unitary matrix $\mathbf{U}$. However, it is difficult to minimize the energy E directly respect to the matrix $\mathbf{U}$. Instead, the matrix $\mathbf{U}$ is usually expanded with an anti-symmetric matrix $\mathbf{R}$, as

$$\mathbf{U} = 1 + \mathbf{R} + \frac{1}{2}\mathbf{R}^2 + \cdots \tag{15}$$

in which $R_{ij} = -R_{ji}$. In some implementations of the CASSCF method such as the first-order super-CI method,[52–59] MOs are optimized by minimizing the total energy E with respect to the non-redundant elements of $\mathbf{R}$.

In the Kylin 1.0 package, we implement the efficient Werner-Meyer-Knowles (WMK) method[60–64] in our program to combine efficient orbital optimizations with FCI as well as DMRG-CI. In the WMK method, the total energy E is expanded to its second order as

$$\begin{aligned} E^{(2)} =& E_0 + 2\sum_{kl} \langle \Delta k|\hat{h}|l\rangle \gamma_{kl} + \sum_{kl} \langle \Delta k|\hat{h}|\Delta l\rangle \gamma_{kl} \\ &+ \sum_{klmn} \left[2\left(\Delta mn|kl\right)\Gamma_{mnkl} + \left(\Delta m\Delta n|kl\right)\Gamma_{mnkl} + 2\left(\Delta mk|l\Delta n\right)\Gamma_{mknl}\right] \end{aligned} \tag{16}$$

in which the first and the second derivatives of MO integrals can be computed explicitly with the unitary matrix $\mathbf{U}$, or, with the auxiliary matrix $\mathbf{T} = \mathbf{U} - \mathbf{1}$ for more convenience. Eq. 16 shows that the total energy E can be expanded to the second order of the matrix $\mathbf{U}$, which, as we can refer to Eq. 15, implies that the total energy E is expanded to the infinite order of the matrix $\mathbf{R}$. Then the anti-symmetric matrix $\mathbf{R}$ can be evaluated by minimizing the functional of the second-order energy $E^{(2)}$ in Eq. 16 with the augmented-Hessian method.[65–69] Near the final solution, the WMK methods achieve quadratic convergence of the energies obtained in successive macro-iterations, which usually leads to less macro-itrations than other CASSCF implementations.

As the DMRG method can be considered as an approximate solution to FCI and CASCI for large active spaces, it is straightforward to implement the DMRG-SCF method by combining DMRG procedures with orbital optimizations.[70,71] Because of the heavy computational costs of DMRG method when applied to large active spaces, it brings significant improvements to use WMK method in DMRG-SCF implementation to make use of its fast convergence. Compared with the CASSCF method, in DMRG-SCF the CI energy and RDMs are generated from spin-adapted DMRG calculations. Besides, the orbital rotation between each pair of active orbitals is not redundant and needs to be precisely evaluated. Other than that, procedures in DMRG-SCF are similar to those in CASSCF.

2.4 MRCI

Despite the CASCI/CASSCF can cover a major part of the electron correlation energy, called static correlation energy, beyond the HF method, the rest missing electron correlation outside the active space still results in quantitative or even qualitative errors for the electronic

structure descriptions of strongly correlated systems. This missing part is named dynamic correlation energy and usually treated by the pos-CAS methods or multi-reference (MR) methods.

The uncontracted multi-reference CI (UC-MRCI) is simplest MR-method. It considers the total configurations within the "first-order-interacting space" (FOIS)[72], and treats them just like CASCI or FCI, thus it has the exponential growth of configurations and makes the final Hamiltonian matrix unsolvable for most molecular systems.

There are two widely used contraction schemes in practice to overcome the exponential growth of configurations in UC-MRCI, the internal contraction (IC)[73–77] and the external contraction (EC)[78]. The IC-MRCI contracts the configurations by simply applying the pair excitation operators on the reference state, and it requires the pre-calculation of high order RDMs in the active space which is computationally challenging for large CAS.

The EC-MRCI doesn't need the calculation of high order RDMs in contrast to IC-MRCI, and it groups together configurations with same internal parts and freezes their relative weights. For example, the single excited states are formed like this:

$$|\psi_S\rangle = \sum_a \alpha_a^S(I)|\phi_S^a(I)\rangle = \sum_a \alpha_t^a(I)|\phi_t^a(I)\rangle, \tag{17}$$

with the EC contraction. Here α coefficients are determined from first-order PT:

$$\alpha_a^S(I) = \frac{\langle\psi_0|\hat{H}|\phi_S^a(I)\rangle}{E_0 - \langle\phi_S^a(I)|\hat{H}|\phi_S^a(I)\rangle} \tag{18}$$

where $|\psi_0\rangle = \sum_I c(I)|\phi(I)\rangle$ is the reference wave function and E_0 indicates the corresponding reference energy, and every S/P denotes a particular internal(N-1)- /(N-2)-electron configuration.

Since DMRG can be regarded as an approximate FCI solver to large active space, the DMRG-EC-MRCI[79] which combines DMRG and EC-MRCI is also available in Kylin 1.0. By ultilizing entropy-driving genetic algorithm (EDGA)[80], in which the selected-CI calculation is performed by using only the leading configurations in the reconstructed wavefunction, DMRG wavefunction can be converted to an approximated wavefunction in configuration bases.

The efficient UC-MRCI and EC-MRCI with or without DMRG codes now can be performed in Kylin 1.0 package. Considering the the deficiency of size-inconsistency in truncated

CI methods, several different correction schemes are also available in Kylin 1.0 package, including Davidson correction,[81] renormalized Davidson correction,[82] Pople correction,[83,84] Duch-Diercksen correction[85] and Meissner correction.[84]

2.5 MRPT

MRPT with a better balance between the computational accuracy and computational costs is probably the most widely used MR-methods nowadays. Since the choice of zeroth-order Hamiltonian $\hat{H}_0$ leads to different perturbation theories, there are various MRPT approaches. The generalized Fock operator, Dyall Hamiltonian, Epstein-Nesbet partition and Fink's Hamiltonian lead to complete active space with second-order perturbation theory (CASPT2)[86–88], second-order N-electron valence state perturbation theory (NEVPT2)[89], second-order Epstein-Nesbet perturbation theory (ENPT2)[90,91] and retaining the excitation degree-PT (REPT)[92]methods respectively.

The multi-reference ENPT2 method is implemented in Kylin 1.0, where the $\hat{H}_0$ is chosen to be:

$$\hat{H}_0 = \sum_{ij\in\Pi} \langle D_i|\hat{H}|D_j\rangle |D_i\rangle\langle D_j| + \sum_{a\notin\Pi} \langle D_a|\hat{H}|D_a\rangle |D_a\rangle\langle D_a|. \tag{19}$$

Here, Π is the variational space spanned by configurations labeled $|D_i\rangle$ and $|D_j\rangle$ in active space, and the rest of this space, spanned by configurations labeled $|D_a\rangle$.

Many other MRPT methods have been integrated with DMRG and provided fruitful DMRG-MRPT approaches, such as DMRG-fully internally contracted (FIC)-CASPT2[93,94], DMRG-strongly contracted (SC)-NEVPT2[95] and MPS-PT[96–99] methods. In Kylin 1.0, the combination of DMRG and MR-ENPT2 is implemented[100], similar in essence to DMRG-EC-MRCI. The solution of a selected CI calculation sampling important configurations(D_i/D_j) is used for building the zeroth-order reference wavefunction in the ENPT2 calculation.

3 TECHNICAL FEATURES

3.1 Geometry Optimization

Geometry optimization is an essential component for an *ab-initio* quantum chemistry software package, which has been widely used in most computational chemistry studies concerning the structure and/or reactivity of molecules. For large systems, efficient geometry optimization relies on the availability of analytical *ab-initio* energy gradient techniques. In the Kylin 1.0 package, the first-order derivative of CASSCF energy is obtained through the following formula[101]:

$$\frac{dE}{da} = \sum_{pq} \gamma_{pq} \frac{dh_{pq}}{da} + \sum_{pqrs} \Gamma_{pqrs} \frac{dv_{pqrs}}{da} - 2 \sum_{pq} \sum_{i \geq j} \left(1 - \frac{\delta_{ij}}{2}\right) C_p^i C_q^j X_{ji} \frac{dS_{pq}}{da} \tag{20}$$

where a is a nuclear coordinate and X is a Lagrange multiplier[102] or generalized Fock operator matrix[103]. It should be noted that $pqrs$ denote the AO indices while ij denote the MOs.

Based on this gradient, quasi-Newton steps are performed to locate stationary points on potential energy surfaces (equilibrium or transition state geometry), where a scaled identity matrix is selected as a guess to an initial Hessian matrix and then, its inverse is updated via the Broyden-Fletcher-Goldfarb-Shanno (BFGS) formula.[104] In case of exceptionally large or small Newton steps, a cubic interpolation method proposed by Davidon[105] is used in the exact line search procedure of each quasi-Newton step. In addition, the algorithm of conjugate gradients[105] is also implemented as an optional optimization method.

3.2 Parallel Execution

Nowadays, the multi-core architecture is widely used on both the personal computer processors and super-computer server processors. To make fully use of the computational capability of this multi-core architecture, an efficient parallel implementation is indispensable. Many parallel algorithms have been developed in a wide range of quantum chemistry methods including the Hartree-Fock method[106], the CI method[107], the coupled-cluster (CC) method[108], and also the DMRG method[29].

In the current stage of the Kylin package, the parallelization optimization is mainly focused on the DMRG process. This parallelization is implemented within the shared memory

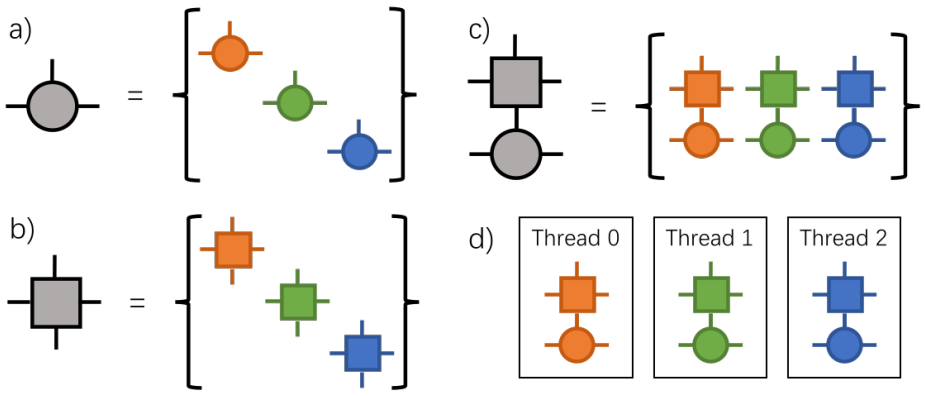

Figure 3: The implemented parallelization algorithm for the DMRG method in the multi-thread level. The block sparse tensor form of the MPS and MPO are illustrated respectively as a) and b). The contraction operation should be conducted for the corresponding MPS and MPO with the same spin symmetry. So the required contraction operations are packed and reordered into a task list as presented as c). Figure d) shows that required operations are assigned to different threads to be processed simultaneously.

programming model. Several parallelism of the DMRG process have been applied to implement this parallelized algorithm include the parallelism within matrix operations, parallelism over symmetry sectors, operators and sum of sub-Hamiltonians. The parallelism within matrix operations is conducted through linking the matrix operations with the linear algebra libraries such as the BLAS library or the MKL library. Besides block-sparse formats, tensors $W^{n_i^* n_i}_{b_{i-1} b_i}$ in MPOs are implemented as a sparse matrices containing one-site operators. Parallelism over symmetry sectors, operators and sub-Hamiltonians could be achieved by simply paralleling over all groups of dense tensor blocks with their corresponding matrix indices and symmetry sectors matched. As the MPOs and MPSs are stored and manipulated within the block-sparse tensor form, those dense blocks can be processed simultaneously with no dependence between each other. Fig. 3 illustrates this parallel implementation, showing the block-sparse tensor and the parallelization of the calculations for corresponding contraction operations.

3.3 Mixed precision

Mixed precision optimization is an emerging method for accelerate quantum chemistry methods, include the integral evaluation[109,110], the SCF iteration[111] and the CC method[112]. Previous works showed that using single-precision instead of double precision can achieve a better computational efficiency while maintaining the chemical accuracy. With some double-precision clean-up process, the double-precision accuracy may also be preserved.

Recently a mixed-precision implementation that can improve the computational performance of the DMRG method and maintain the double-precision accuracy was introduced and implemented within the Kylin package[113]. This implementation is based on the idea that the the DMRG method is a iterative method and the first several iterations can be evaluated in a relatively low precision. Followed with a double-precision clean-up procedure, the double-precision accuracy can be successfully recovered. To make the single-precision DMRG generate reasonably approximate solutions, the orthogonalization process should be conducted in double-precision as the Gram-Schmidt process may be numerically unstable. Also within the double-precision clean-up procedure, a mixed-precision diagonalization method is applied to achieve a better performance, constructing a two-level mixed-precision hierarchy.

4 NUMERICAL EXAMPLES AND DISCUSSIONS

In this section, we show some typical multi-configurational quantum chemical calculations performed with Kylin 1.0. The molecular geometries used in this section are shown in Figure 4.

Firstly, we test DMRG-FCI (10e, 58o) calculations for water molecules under the equilibrium geometry ($r_{\mathrm{OH}} = r_e$) and a stretched geometry where the OH bond is stretched to 1.5 times its equilibrium length ($r_{\mathrm{OH}} = 1.5\ r_e$). The detailed molecular structures are taken from the earlier work by Chan and Head-Gordon[114]. We use the cc-pVTZ (correlation consistent-polarized valence triple zeta) basis set and then perform a FCI calculation for correlating 10 electrons in all 58 orbitals by DMRG. Fig. 5 illustrates the dependence of DMRG ground state energy on the size parameter of its wavefunction's basis set (bond-dimenision number

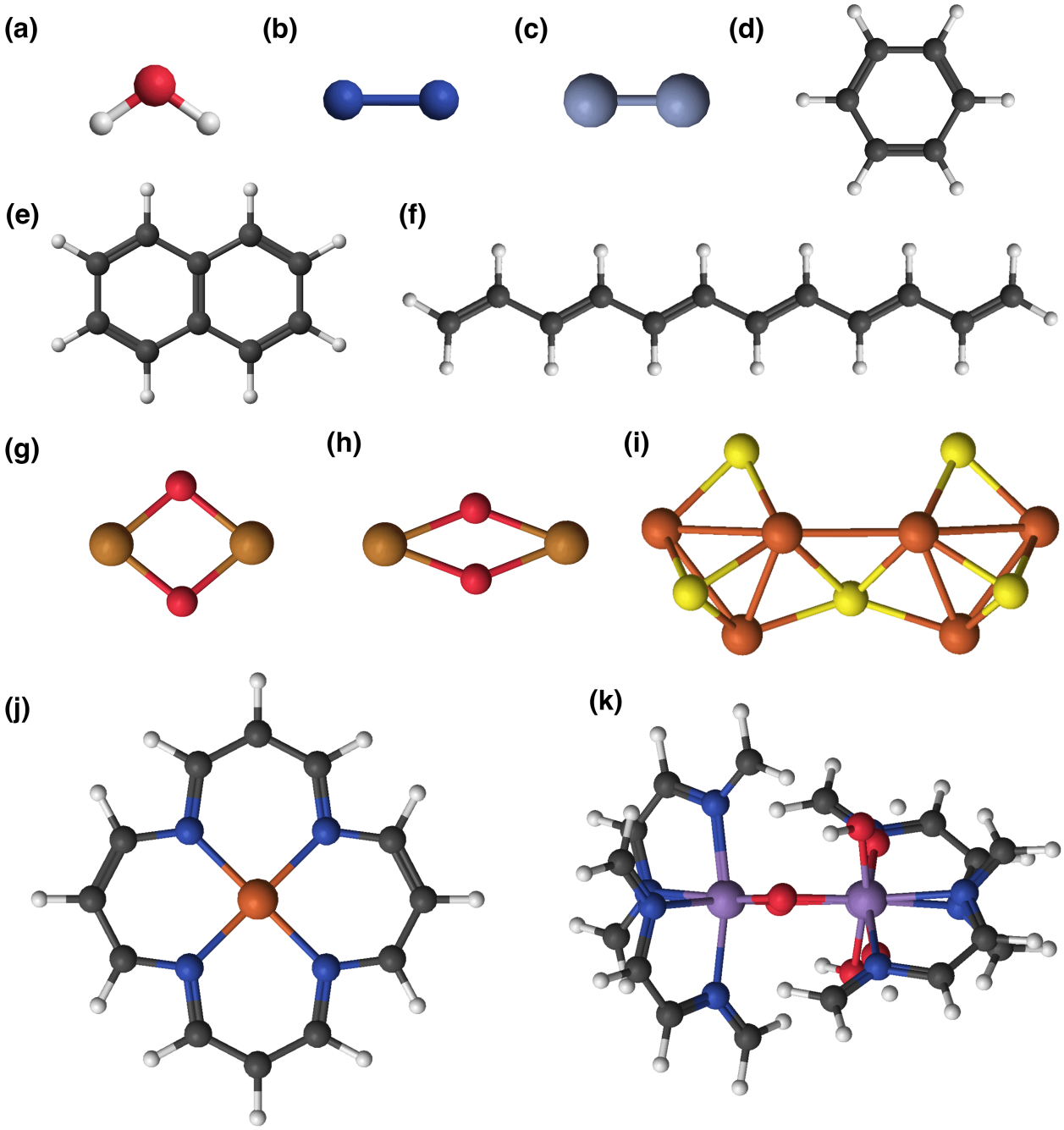

Figure 4: The molecular geometries used in this work. They are (a) water, (b) N_2, (c) Cr_2, (d) benzene, (e) naphthalene, (f) $C_{12}H_{14}$ polyacetylene, (g) bis(μ-oxo)-$Cu_2O_2^{2+}$, (h) peroxo-$Cu_2O_2^{2+}$, (i) Fe_8S_7 cluster, (j) Fe-porphyrin and (k) $[(Mn)_3O_4L_4(H_2O)_2]$ (L = N,N$'$-bis(methylene)-Z-1,2-ethenediamine).

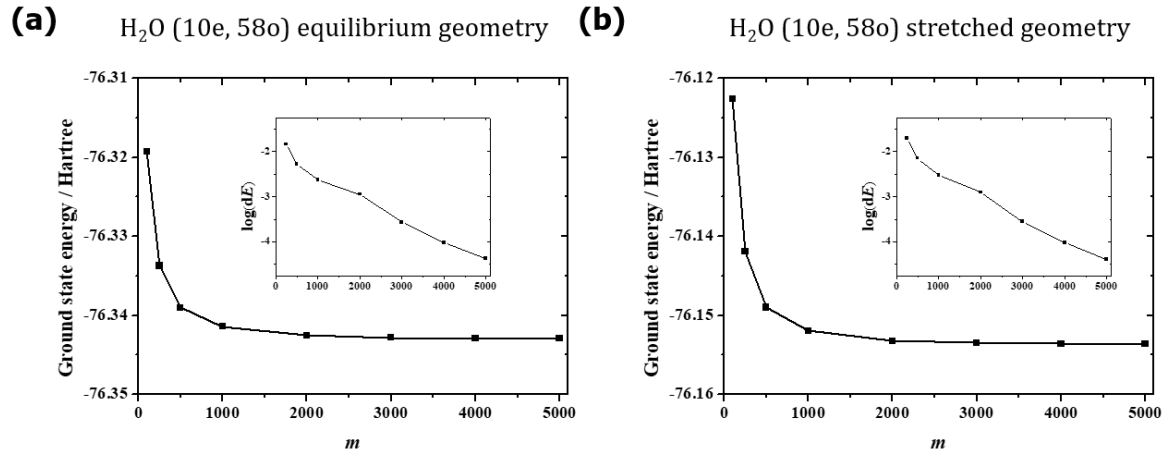

Figure 5: The ground state energies of water molecules with (a) $r_{\mathrm{OH}} = r_e$ and (b) $r_{\mathrm{OH}} = 1.5\ r_e$ calculated by DMRG(10e, 58o) with different bond-dimenision numbers (m). dE is calculated as the energy difference between the energy by DMRG with the current m and that by DMRG with previous m.

m). It is clearly shown that the DMRG energy decreases monotonically with the increasing m, converging to the final FCI solution. The insets of Fig. 5 indicate that the energy variation with the increasing m has become less than 1×10^{-4} Hartree. Considering the variational nature for DMRG, we compare DMRG energies with results by other variational approaches. One may notice that, DMRG calculations with sufficiently large m will yield (much) lower ground state energies when compared to those by CISD, which are -76.30994 and -76.10233 Hartree for the equilibrium and stretched geometries respectively. This verifies again that DMRG can provide a powerful computational tool for very accurate electronic structure calculations within a finite active space composing of a few tens of orbitals.

Secondly, we show Kylin 1.0's CASSCF functionality by numerical examples of two medium-sized naphthalene and $C_{12}H_{14}$ molecules. The equilibrium geometries of these two molecules are optimized by density functional theory (DFT) at the level of B3LYP/cc-pVDZ by using Gaussian16 software[115]. We then perform CASSCF calculations with the same basis set (sizes of 180 and 238 for naphthalene and $C_{12}H_{14}$ respectively) and the π-electrons and π-orbitals are chosen as the active spaces, i.e. (10e, 10o) and (12e, 12o) for naphthalene and $C_{12}H_{14}$ respectively. As we have introduced in the methodology section, Kylin 1.0 adopts the

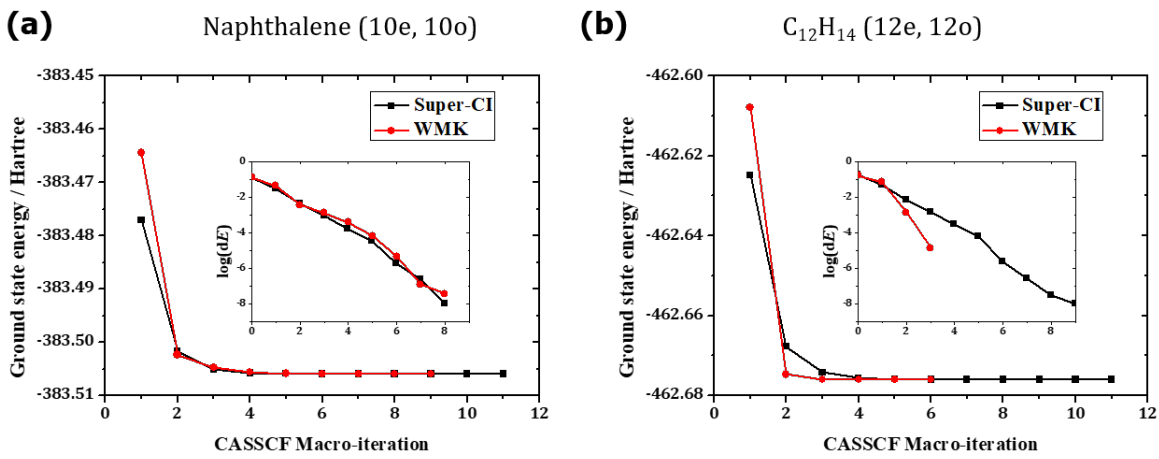

Figure 6: Convergence of CASSCF calculations for the ground states of (a) naphthalene (10e, 10o) and (b) $C_{12}H_{14}$ (12e, 12o) molecules by using different CASSCF algorithms. dE is calculated as the energy difference between the energy at current CASSCF macro-iteration and the finally converged ground state energy by CASSCF.

efficient second-order WMK method[60–64] in our CASSCF implementation. For comparison, CASSCF calculations based on the first-order super-CI algorithm are also performed by using OpenMolcas[34] as references. One can clearly see from Fig. 6 that, the calculations by the two different CASSCF algorithms in Kylin and OpenMolcas converge to exactly the same ground state energy results, verifying the correctness of our WMK-CASSCF functionality in Kylin 1.0. It is also obvious in the insets of Fig. 6 that the convergence efficiency by the WMK algorithm is generally comparable to that of the super-CI algorithm. In the slightly larger system of $C_{12}H_{14}$ (12e, 12o), WMK converges even faster than super-CI because of its second-order nature.

Next, we show Kylin 1.0's DMRG-SCF functionality, which integrates DMRG's advantage of dealing with large active spaces and CASSCF's feature of orbital optimization. Here we take the interconversion between the bis(μ-oxo) and peroxo forms of dicopper complexes with a $Cu_2O_2^{2+}$ core as a numerical example, which is crucial in oxyhemocyanin and oxytyrosinase in biological catalysis. We employ the ANO-RCC basis sets, and the scalar relativistic corrections are included by adopting the Douglas-Kroll-Hess Hamiltonian. The detailed molecular structures are taken from the earlier work by Phung, et al.[116] We choose a (24e,

24o) active space for $Cu_2O_2^{2+}$ core, including the most important correlation effects related to the Cu−O bonds and the Cu $3d$ double-shell effect, consisting of twenty Cu orbitals ($3d$, $3d'$) and four O orbitals ($2p_x$, $2p_y$). It was shown that the ground-state energy of peroxo structure of $Cu_2O_2^{2+}$ is lower than bis(μ-oxo) structure, and the relative energy can reach convergence gradually with the growth of m value.

Table 1: The ground-state energies of the bis(μ-oxo) and peroxo structures of $Cu_2O_2^{2+}$ in unit of Hartree and their differences in unit of kcal·mol^{-1} calculated by DMRG-SCF (24e, 24o) with different m values.

m	E(bis(μ-oxo))	E(peroxo)	ΔE
100	-3455.573778	-3455.673656	62.67
200	-3455.662490	-3455.745492	52.08
400	-3455.708920	-3455.783380	46.72
1000	-3455.730964	-3455.803941	45.79
1500	-3455.752671	-3455.813994	38.48
2000	-3455.758435	-3455.8194004	38.26
2500	-3455.761956	-3455.822788	38.17

To benchmark the performance of our parallel implementation of the DMRG method, we test DMRG calculations for the Fe-porphyrin system ($m = 5000$). The molecular geometry is taken from Li Manni's work.[117] We use the same (32e, 34o) active space as Weser and co-workers used before,[118] which consists of all π orbitals, the four σ_N orbitals connecting to the Fe atom, the $4s$, $4p$ and $3d$ orbitals of the Fe atom, and an additional set of d orbitals as the double-shell. The ANO-RCC-VDZP basis set[119,120] is used in our calculations. The computing platform is a standalone server containing two Intel Xeon Gold 6126 12-core CPUs. The total DMRG calculation time for different number of threads are presented in Fig. 7 with corresponding speed-up comparing to the time of 1 thread. A speed-up of up to 10.05 is observed for 24 threads, giving a 41.9% parallel efficiency. This parallel performance is moderately satisfactory by considering the irregular data distribution for the block-sparse tensor in DMRG and we believe this parallel efficiency can be improved with further optimizations like improving the load balance and reducing the cache-miss rate.

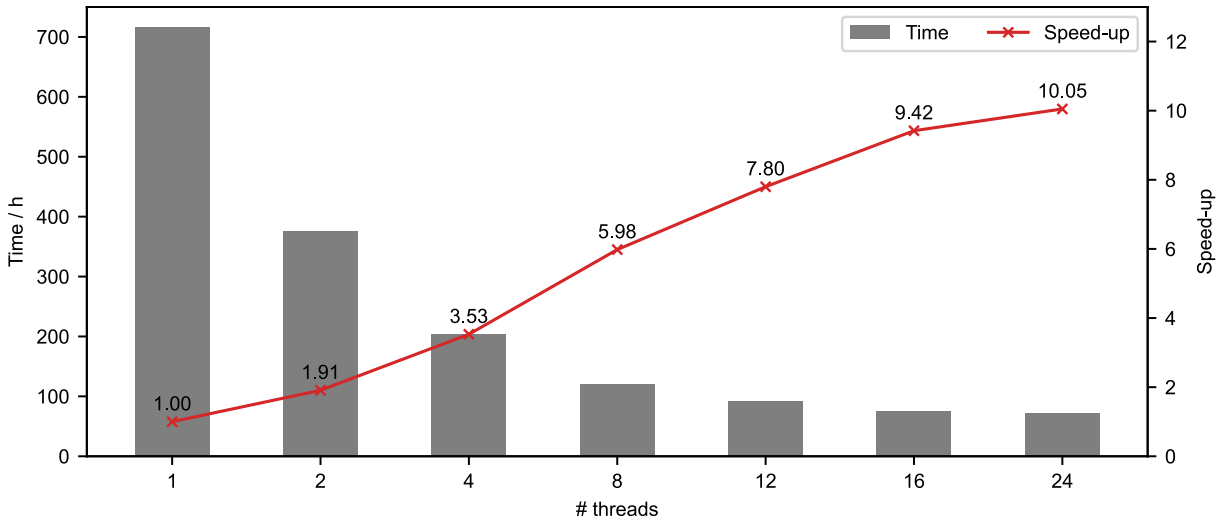

Figure 7: Benchmark results of computational time and speed-up for parallel DMRG calculation with Fe-porphyrin (32e, 34o) with m=5000.

Also, we have planned to develop a hybrid parallel algorithm, combining the shared-memory model and distributed-memory model, with more parallelism involved to achieve a better parallel efficiency.

Furthermore, we test the computational performance of our mixed-precision implementation in the DMRG module. The selected benchmark systems are N_2, benzene, Fe-porphyrin and Fe_8S_7 cluster systems with active spaces containing up to 114 active orbitals. The detailed information of these benchmark systems and the energy difference between the mixed-precision implementation and the double-precision calculation are summarized in Tabel 2. It can be found that, for these different cases with different basis set and point group symmetries, the energy errors caused by the mix-precision approximation are mostly much lower than 1 kcal·mol^{-1}, which is commonly regarded as the chemical accuracy. The benchmark results of computational time performance are presented in Fig. 8. The result shows that for different basis sets and point group symmetries with relatively large truncation dimension, the mixed-precision implementation can perform much faster than the double-precision version. And the speed-up is achieved up to 2.31, which is even larger than the theoretical upper-bond of the mixed-precision optimization. This is because of two reasons. The first

Table 2: Detailed information of the benchmark system and the energy difference for the mixed-precision implementation. The energy difference is evaluated as $\Delta E = |E_{\text{double}} - E_{\text{mix}}|$ in 10^{-3} kcal·mol^{-1}.

System	basis set	active space	m	point group	ΔE
N_2	cc-pVDZ	(14e, 28o)	3000	C_1	11.9
benzene	6-31G	(24e, 24o)	5000	C_1	0.5
benzene	cc-pVDZ	(42e, 114o)	1000	D_{2h}	10.9
Fe-porphyrin	ANO-RCC-VTZP	(32e, 34o)	3000	C_1	89.0
Fe_8S_7	ANO-RCC-VTZP	(168e, 100o)	1000	C_{2v}	75.4

reason is that the single-precision floating-point data consumes less memory than double-precision, which means that more data can be stored in the cache and the cache-miss rate is reduced. The second reason is the total number of sweep iteration is reduced for some cases. So that the overall computational time is further reduced.

But for the benzene (42e, 114o) case, the mixed-precision implementation shows no acceleration, even slightly slower than double precision. This is because, for this specific case, the tensor contraction is not the bottle neck. The task packing process, which matches corresponding block tensors together for further contraction, become the most time consuming step. And this step consumes similar time between double precision and mixed precision.

More benchmark results and discussions for the mixed-precision scheme can be found in our recent work[113]. In short, here we show that the mixed-precision implementation provides an efficient speed-up strategy with the price of vanishingly small numerical errors, which is highly beneficial to the generally expensive DMRG calculations for large strongly correlated systems.

Finally, we show Kylin 1.0's DMRG-EC-MRCI functionality, which can descibe the static correlation inside the large active space and the dynamic correlation outside the active space simultaneously. Since high-valent multinuclear oxomanganese complexes are crucial in photosystem II,[121] we use $[(Mn)_3O_4L_4(H_2O)_2]$ (shown in Figure 4(k)) as an example, with L = N,N′-bis(methylene)-Z-1,2-ethenediamine. It is a simplified system of $[(Mn)_3O_4(bpy)_4(H_2O)_2]^{4+}$ (bpy = 2,2'-bipyridine), which has been experimentally deter-

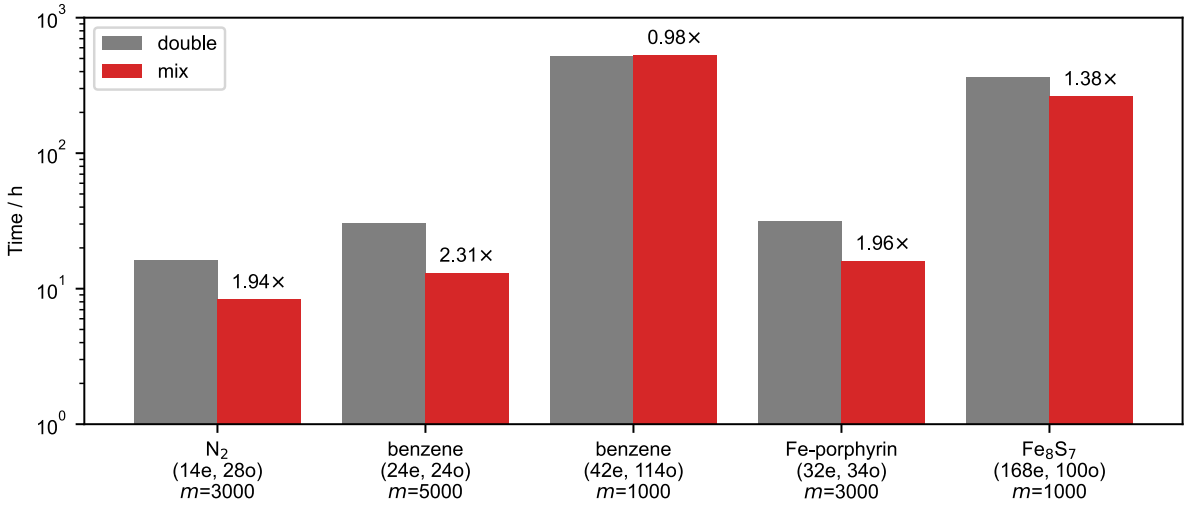

Figure 8: Benchmark result of computational time and corresponding speed-up for mixed-precision implementation comparing to double precision. Note that the time is presented in logarithmic coordinate

mined to have an energy difference of -0.2 kcal·mol^{-1} between low spin (LS) ground state ($S = 1/2$) and high spin (HS) first excited state ($S = 3/2$).[122]

The geometry of $[(Mn)_3O_4L_4(H_2O)_2]$ is taken from Ref[123], for both LS and HS state calculations. The scalar relativistic corrections are included by adopting the X2C[124,125] Hamiltonian. The ANO-RCC-VDZP basis set is used for Mn, while the ANO-RCC-VDZ and ANO-RCC-MB basis sets are used for O, N and C, H respectively. The active space (43e, 34o) are constructed by atomic valence active space (AVAS) scheme[126] using Beijing Density Functional (BDF) package (development version)[127], selecting 3d, 4s of Mn and 2p of bridging O based on HS state ROHF orbitals with ANO-RCC-MB as minimal basis set and overlap threshold larger than 0.2. The DMRG-CI calculations are performed with $M = 1000$. The EC-MRCISD+Q (with renormalized Davidson correction[82]) calculations are performed using truncated reference wavefunctions constructed via EDGA[80] with CI completeness of 0.90. The core orbitals are frozen in EC-MRCISD+Q calculation.

The calculated energy difference is listed in Table 3. It can be found that there has been a sharp decrease of energy difference from DMRG-CI (-10.8 kcal·mol^{-1}) to DMRG-EC-MRCISD+Q (-0.3 kcal·mol^{-1}), which is in excellent agreement with experiment value.

Table 3: Energy difference of LS and HS states for $[(Mn)_3O_4L_4(H_2O)_2]$ (L = N,N′-bis(methylene)-Z-1,2-ethenediamine). The energy difference is calculated as $\Delta E = E_{\mathrm{LS}} - E_{\mathrm{HS}}$ in kcal·mol^{-1}. The experiment value is taken from Ref[122] for $[(Mn)_3O_4(bpy)_4(H_2O)_2]^{4+}$ (bpy = 2,2'-bipyridine). The DFT energy difference is take from Ref[123] at B3LYP level, with basis sets LACVP for Mn, 6-31G(d) for O, 6-31G for N as well as 3-21G for C and H.

	Experiment	DFT	DMRG-CASCI	DMRG-EC-MRCISD+Q
ΔE	-0.2	21.0	-10.8	-0.3

The significant improvement over DMRG is contributed by the consideration of dynamic correlation by MRCI and this clearly shows post-DMRG's powerful ability of quantitative description of electronic structure properties.

5 CONCLUSIONS

The present paper introduces a new *ab-initio* DMRG quantum chemistry software package, Kylin 1.0, which contains versatile DMRG (DMRG-CI, DMRG-SCF) and pre-DMRG (Hartree-Fock SCF), post-DMRG (DMRG-MRCI and DMRG-MRPT) modules as well as other fundamental ones (CI, PT, CASSCF). Numerical examples of various conjuagted and stretched molecules as well as transition metal complexes have shown that by virtue of using Kylin 1.0, state-of-art DMRG calculations with more than 100 active orbitals and post-DMRG calculations with more than 40 active orbitals can be efficiently implemented at a standalone computer server. It's also worth to note that, Kylin 1.0 is an independent quantum chemical software package, and accordingly additional interfaces to other quantum chemical packages are avoided. Therefore, Kylin 1.0 provides a new, convenient, efficient and powerful DMRG quantum chemistry platform for electronic structure calculations of large strongly correlated molecules. In order to popularize *ab-initio* DMRG calculations in more real chemistry or material applications at highly quantitative levels, future developments will certainly, to some extent, feature new post-DMRG methods without using high-order RDMs and periodic DMRG as well as post-DMRG calculations with/without the relativistic effect.

6 ACKNOWLEDGMENTS

This work was supported by the National Natural Science Foundation of China (Grant 22073045), the Fundamental Research Funds for the Central Universities and the program B for Outstanding PhD candidate of Nanjing University.

References

1. J. W. Park, R. Al-Saadon, M. K. MacLeod, T. Shiozaki, and B. Vlaisavljevich, Chem. Rev. **120**, 5878 (2020).

2. H. Lischka, D. Nachtigallova, A. J. Aquino, P. G. Szalay, F. Plasser, F. B. Machado, and M. Barbatti, Chem. Rev. **118**, 7293 (2018).

3. C. Hattig, W. Klopper, A. Kohn, and D. P. Tew, Chem. Rev. **112**, 4 (2012).

4. P. G. Szalay, T. Muller, G. Gidofalvi, H. Lischka, and R. Shepard, Chem. Rev. **112**, 108 (2012).

5. D. I. Lyakh, M. Musiał, V. F. Lotrich, and R. J. Bartlett, Chem. Rev. **112**, 182 (2012).

6. G. H. Booth, A. J. Thom, and A. Alavi, J. Chem. Phys. **131**, 054106 (2009).

7. B. Huron, J. Malrieu, and P. Rancurel, J. Chem. Phys. **58**, 5745 (1973).

8. A. A. Holmes, N. M. Tubman, and C. Umrigar, J. Chem. Theory Comput. **12**, 3674 (2016).

9. S. Sharma, A. A. Holmes, G. Jeanmairet, A. Alavi, and C. J. Umrigar, J. Chem. Theory Comput. **13**, 1595 (2017).

10. W. Liu and M. R. Hoffmann, J. Chem. Theory Comput. **12**, 1169 (2016).

11. Y. Guo, N. Zhang, Y. Lei, and W. Liu, J. Chem. Theory Comput. **17**, 7545 (2021).

12. S. R. White, Phys. Rev. Lett. **69**, 2863 (1992).

13. S. R. White, Phys. Rev. B **48**, 10345 (1993).

14. U. Schollwöck, Rev. Mod. Phys. **77**, 259 (2005).

15. U. Schollwöck, Ann. Phys. **326**, 96 (2011).

16. S. R. White and R. L. Martin, J. Chem. Phys. **110**, 4127 (1999).

17. S. Daul, I. Ciofini, C. Daul, and S. R. White, Int. J. Quantum Chem. **79**, 331 (2000).

18. G. K.-L. Chan and M. Head-Gordon, J. Chem. Phys. **116**, 4462 (2002).

19. A. O. Mitrushenkov, G. Fano, F. Ortolani, R. Linguerri, and P. Palmieri, J. Chem. Phys. **115**, 6815 (2001).

20. S. Keller, M. Dolfi, M. Troyer, and M. Reiher, J. Chem. Phys. **143**, 244118 (2015).

21. S. Keller and M. Reiher, J. Chem. Phys. **144**, 134101 (2016).

22. H. Ma, U. Schollwöck, and Z. Shuai, Density Matrix Renormalization Group (DMRG)-based Approaches in Computational Chemistry (Elsevier, 2022).

23. G. K.-L. Chan and D. Zgid, Annu. Rep. Comput. Chem. **5**, 149 (2009).

24. Y. Kurashige, Mol. Phys. **112**, 1485 (2014).

25. S. Wouters and D. Van Neck, Eur. Phys. J. D **68**, 272 (2014).

26. A. Baiardi and M. Reiher, J. Chem. Phys. **152**, 040903 (2020).

27. L. Freitag and M. Reiher, The Density Matrix Renormalization Group for Strong Correlation in Ground and Excited States (John Wiley & Sons, Ltd, 2020), chap. 7, pp. 205–245.

28. Y. Cheng, Z. Xie, and H. Ma, J. Phys. Chem. Lett. **13**, 904 (2022).

29. H. Zhai and G. K.-L. Chan, J. Chem. Phys. **154**, 224116 (2021).

30. S. Knecht, E. Hedegård, S. Keller, A. Kovyrshin, Y. Ma, A. Muolo, C. Stein, and M. Reiher, Chimia **70**, 244 (2016).

31. S. Wouters, W. Poelmans, P. W. Ayers, and D. Van Neck, Comput. Phys. Commun. **185**, 1501 (2014).

32. Q. Sun, T. C. Berkelbach, N. S. Blunt, G. H. Booth, S. Guo, Z. Li, J. Liu, J. D. McClain, E. R. Sayfutyarova, S. Sharma, et al., Wiley Interdiscip. Rev. Comput. Mol. Sci. **8**, e1340 (2018).

33. Q. Sun, X. Zhang, S. Banerjee, P. Bao, M. Barbry, N. S. Blunt, N. A. Bogdanov, G. H. Booth, J. Chen, Z.-H. Cui, et al., J. Chem. Phys. **153**, 024109 (2020).

34. F. Aquilante, J. Autschbach, A. Baiardi, S. Battaglia, V. A. Borin, L. F. Chibotaru, I. Conti, L. De Vico, M. Delcey, I. Fdez. Galván, et al., J. Chem. Phys. **152**, 214117 (2020).

35. D. Hartree, in Math. Proc. Cambridge Philos. Soc. (Cambridge University Press, 1928), vol. 24, pp. 89–110.

36. J. C. Slater, Phys. Rev. **35**, 210 (1930).

37. C. C. J. Roothaan, Rev. Mod. Phys. **23**, 69 (1951).

38. Q. Sun, J. Comput. Chem. **36**, 1664 (2015).

39. J. Stewart, P. Császár, and P. Pulay, J. Comput. Chem. **3**, 227 (1982).

40. H. Sellers, Int. J. Quantum Chem. **45**, 31 (1993).

41. K. N. Kudin, G. E. Scuseria, and E. Cances, J. Chem. Phys. **116**, 8255 (2002).

42. E. R. Davidson, J. Chem. Phys. **62**, 400 (1975).

43. I. Shavitt, Int. J. Quantum Chem. **14**, 5 (1978).

44. I. Shavitt, Chem. Phys. Lett. **63**, 421 (1979).

45. B. R. Brooks and H. F. Schaefer, J. Chem. Phys. **70**, 5092 (1979).

46. B. R. Brooks, W. D. Laidig, P. Saxe, N. C. Handy, and H. F. Schaefer, Phys. Scr. **21**, 312 (1980).

47. J. Paldus, in The Unitary Group for the Evaluation of Electronic Energy Matrix Elements, edited by J. Hinze (Springer Berlin Heidelberg, Berlin, Heidelberg, 1981), pp. 1–50.

48. I. Shavitt, in The Unitary Group for the Evaluation of Electronic Energy Matrix Elements, edited by J. Hinze (Springer Berlin Heidelberg, Berlin, Heidelberg, 1981), pp. 51–99.

49. B. Roos, Chem. Phys. Lett. **15**, 153 (1972).

50. B. O. Roos and P. E. M. Siegbahn, in Methods of Electronic Structure Theory, edited by H. F. Schaefer (Springer US, Boston, MA, 1977), pp. 277–318.

51. C. Møller and M. S. Plesset, Phys. Rev. **46**, 618 (1934).

52. F. Grein and T. Chang, Chem. Phys. Lett. **12**, 44 (1971).

53. F. Grein and A. Banerjee, Int. J. Quantum Chem. **9**, 147 (1975).

54. B. O. Roos, P. R. Taylor, and P. E. Sigbahn, Chem. Phys. **48**, 157 (1980).

55. B. O. Roos, Int. J. Quantum Chem. **18**, 175 (1980).

56. P. Siegbahn, A. Heiberg, B. Roos, and B. Levy, Phys. Scr. **21**, 323 (1980).

57. P. E. Siegbahn, J. Almlöf, A. Heiberg, and B. O. Roos, J. Chem. Phys. **74**, 2384 (1981).

58. B. O. Roos, in Methods in Computational Mol. Phys. (Springer, 1983), pp. 161–187.

59. P. Å. Malmqvist, A. Rendell, and B. O. Roos, J. Phys. Chem. **94**, 5477 (1990).

60. H.-J. Werner and W. Meyer, J. Chem. Phys. **73**, 2342 (1980).

61. H.-J. Werner and P. J. Knowles, J. Chem. Phys. **82**, 5053 (1985).

62. P. J. Knowles and H.-J. Werner, Chem. Phys. Lett. **115**, 259 (1985).

63. H.-J. Werner, Adv. Chem. Phys. **69**, 1 (1987).

64. D. A. Kreplin, P. J. Knowles, and H.-J. Werner, J. Chem. Phys. **150**, 194106 (2019).

65. B. H. Lengsfield III, J. Chem. Phys. **73**, 382 (1980).

66. B. H. Lengsfield III and B. Liu, J. Chem. Phys. **75**, 478 (1981).

67. R. Shepard, I. Shavitt, and J. Simons, J. Chem. Phys. **76**, 543 (1982).

68. P. Jørgensen, P. Swanstrom, and D. L. Yeager, J. Chem. Phys. **78**, 347 (1983).

69. J. T. Golab, D. L. Yeager, and P. Jørgensen, Chem. Phys. **78**, 175 (1983).

70. Y. Ma, S. Knecht, S. Keller, and M. Reiher, J. Chem. Theory Comput. **13**, 2533 (2017).

71. Q. Sun, J. Yang, and G. K.-L. Chan, Chem. Phys. Lett. **683**, 291 (2017).

72. A. McLean and B. Liu, J. Chem. Phys. **58**, 1066 (1973).

73. W. Meyer, in Methods of Electronic Structure Theory (Plenum Press New York, 1977), vol. 3.

74. P. E. Siegbahn, Int. J. Quantum Chem. **18**, 1229 (1980).

75. H.-J. Werner and E.-A. Reinsch, J. Chem. Phys. **76**, 3144 (1982).

76. H.-J. Werner and P. J. Knowles, J. Chem. Phys. **89**, 5803 (1988).

77. P. J. Knowles and H.-J. Werner, Chem. Phys. Lett. **145**, 514 (1988).

78. P. E. Siegbahn, Int. J. Quantum Chem. **23**, 1869 (1983).

79. Z. Luo, Y. Ma, X. Wang, and H. Ma, J. Chem. Theory Comput. **14**, 4747 (2018).

80. Z. Luo, Y. Ma, C. Liu, and H. Ma, J. Chem. Theory Comput. **13**, 4699 (2017).

81. S. R. Langhoff and E. R. Davidson, Int. J. Quantum Chem. **8**, 61 (1974).

82. W. L. Luken, Chem. Phys. Lett. **58**, 421 (1978).

83. J. Pople, R. Seeger, and R. Krishnan, Int. J. Quantum Chem. **12**, 149 (1977).

84. L. Meissner, Chem. Phys. Lett. **146**, 204 (1988).

85. W. Duch and G. H. Diercksen, J. Chem. Phys. **101**, 3018 (1994).

86. B. O. Roos, P. Linse, P. E. Siegbahn, and M. R. Blomberg, Chem. Phys. **66**, 197 (1982).

87. K. Andersson, P. A. Malmqvist, B. O. Roos, A. J. Sadlej, and K. Wolinski, J. Phys. Chem. **94**, 5483 (1990).

88. K. Andersson, P.-Å. Malmqvist, and B. O. Roos, J. Chem. Phys. **96**, 1218 (1992).

89. C. Angeli, R. Cimiraglia, S. Evangelisti, T. Leininger, and J.-P. Malrieu, J. Chem. Phys. **114**, 10252 (2001).

90. P. S. Epstein, Phys. Rev. **28**, 695 (1926).

91. R. Nesbet, Proc. R. Soc. Lond. A Math. Phys. Sci. **230**, 312 (1955).

92. R. F. Fink, Chem. Phys. **356**, 39 (2009).

93. Y. Kurashige and T. Yanai, J. Chem. Phys. **135**, 094104 (2011).

94. Y. Kurashige, J. Chalupskỳ, T. N. Lan, and T. Yanai, J. Chem. Phys. **141**, 174111 (2014).

95. S. Guo, M. A. Watson, W. Hu, Q. Sun, and G. K.-L. Chan, J. Chem. Theory Comput. **12**, 1583 (2016).

96. S. Sharma and G. K.-L. Chan, J. Chem. Phys. **141**, 111101 (2014).

97. S. Sharma, G. Jeanmairet, and A. Alavi, J. Chem. Phys. **144**, 034103 (2016).

98. S. Sharma, G. Knizia, S. Guo, and A. Alavi, J. Chem. Theory Comput. **13**, 488 (2017).

99. S. Sharma and A. Alavi, J. Chem. Phys. **143**, 102815 (2015).

100. Y. Song, Y. Cheng, Y. Ma, and H. Ma, Electron. Struct. **2**, 014002 (2020).

101. W. Hu and G. K.-L. Chan, J. Chem. Theory Comput. **11**, 3000 (2015).

102. W. Koch, A New Dimension to Quantum Chemistry. Analytic Derivative Methods in Ab Initio Molecular Electronic Structure Theory. Von Y. Yamaguchi, Y. Osamura, JD Goddard und HF Schaefer. Oxford University Press, Oxford, 1994. 471 S., geb. 60.00£.–ISBN 0-19-507028-3 (Wiley Online Library, 1995).

103. J. Hinze, J. Chem. Phys. **59**, 6424 (1973).

104. H. B. Schlegel, Wiley Interdiscip. Rev. Comput. Mol. Sci. **1**, 790 (2011).

105. R. Fletcher and C. M. Reeves, Comput. J. **7**, 149 (1964).

106. G. M. J. Barca, D. L. Poole, J. L. G. Vallejo, M. Alkan, C. Bertoni, A. P. Rendell, and M. S. Gordon, in SC20: International Conference for High Performance Computing, Networking, Storage and Analysis (2020), pp. 1–14.

107. K. D. Vogiatzis, D. Ma, J. Olsen, L. Gagliardi, and W. A. de Jong, J. Chem. Phys. **147**, 184111 (2017).

108. J. Kim, A. Panyala, B. Peng, K. Kowalski, P. Sadayappan, and S. Krishnamoorthy, in SC20: International Conference for High Performance Computing, Networking, Storage and Analysis (2020), pp. 1–15.

109. N. Luehr, I. S. Ufimtsev, and T. J. Martínez, J. Chem. Theory Comput. **7**, 949 (2011).

110. A. Asadchev and M. S. Gordon, Comput. Phys. Commun. **183**, 1563 (2012).

111. R. M. Parrish, F. Liu, and T. J. Martínez, J. Chem. Phys. **144**, 131101 (2016).

112. P. Pokhilko, E. Epifanovsky, and A. I. Krylov, J. Chem. Theory Comput. **14**, 4088 (2018).

113. Y. Tian, Z. Xie, Z. Luo, and H. Ma, J. Chem. Theory Comput. (2022).

114. G. K.-L. Chan and M. Head-Gordon, J. Chem. Phys. **118**, 8551 (2003).

115. M. J. Frisch, G. W. Trucks, H. B. Schlegel, G. E. Scuseria, M. A. Robb, J. R. Cheeseman, G. Scalmani, V. Barone, G. A. Petersson, H. Nakatsuji, et al., Gaussian 16 Revision C.01 (2016), gaussian Inc. Wallingford CT, URL `https://gaussian.com`.

116. Q. M. Phung, S. Wouters, and K. Pierloot, J. Chem. Theory Comput. **12**, 4352 (2016).

117. G. Li Manni and A. Alavi, J. Phys. Chem. A **122**, 4935 (2018).

118. O. Weser, L. Freitag, K. Guther, A. Alavi, and G. Li Manni, Int. J. Quantum Chem. **121**, e26454 (2021).

119. P.-O. Widmark, P.-Å. Malmqvist, and B. O. Roos, Theor. Chim. Acta. **77**, 291 (1990).

120. B. O. Roos, R. Lindh, P.-Å. Malmqvist, V. Veryazov, and P.-O. Widmark, J. Phys. Chem. A **108**, 2851 (2004).

121. S. Mukhopadhyay, S. K. Mandal, S. Bhaduri, and W. H. Armstrong, Chem. Rev. **104**, 3981 (2004).

122. J. E. Sarneski, H. H. Thorp, G. W. Brudvig, R. H. Crabtree, and G. K. Schulte, J. Am. Chem. Soc. **112**, 7255 (1990).

123. E. M. Sproviero, J. A. Gascon, J. P. McEvoy, G. W. Brudvig, and V. S. Batista, J. Inorg. Biochem. **100**, 786 (2006).

124. W. Kutzelnigg and W. Liu, J. Chem. Phys. **123**, 241102 (2005).

125. D. Peng and M. Reiher, Theor. Chem. Acc. **131**, 1081 (2012).

126. E. R. Sayfutyarova, Q. Sun, G. K.-L. Chan, and G. Knizia, J. Chem. Theory Comput. **13**, 4063 (2017).

127. Y. Zhang, B. Suo, Z. Wang, N. Zhang, Z. Li, Y. Lei, W. Zou, J. Gao, D. Peng, Z. Pu, et al., J. Chem. Phys. **152**, 064113 (2020).